Available online at www.sciencedirect.com

ScienceDirect

journal homepage: www.elsevier.com/locate/he

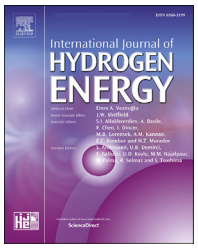

Metallurgical and mechanical properties of hydrogen charged carbide-free bainitic weld metals

Sudharsanan Sundaram [a,*], G D Janaki Ram [b], Murugaiyan Amirthalingam [a]

[a] Department of Metallurgical and Materials Engineering, IIT Madras, JAML, Chennai, 600036, TN, India
[b] Department of Materials Science and Metallurgical Engineering, IIT Hyderabad, Kandi, 502285, TS, India

HIGHLIGHTS

- Volume fraction of retained austenite has a direct correlation with hydrogen saturation.
- Blocky austenite is detrimental in retaining tensile strength after hydrogen saturation.
- Welds without martensite and blocky austenite are least susceptible to hydrogen embrittlement.

ARTICLE INFO

Article history:
Received 13 December 2022
Received in revised form
20 January 2023
Accepted 22 January 2023
Available online 16 February 2023

Keywords:
Hydrogen embrittlement
Carbide-free bainite weld
Nanostructured bainitic steels
Diffusible hydrogen
Retained austenite

ABSTRACT

Hydrogen embrittlement is a major concern during the welding of high-strength steels. The susceptibility of the welds to hydrogen embrittlement increases with increase in weld strength. The ever-increasing demand to increase the strength of steels necessitates the development of novel welding procedures and fillers to produce welds of high strength and with resistance to hydrogen embrittlement. In this current work, the susceptibility of carbide-free bainitic weld metals to hydrogen embrittlement is studied with varying volume fractions of constituent phases. Using three different weld metal compositions, six different weld metal microstructures of carbide-free bainite were generated. The hydrogen saturation behaviour of the various weld metals was studied by cathodic electrolytic charging and subsequent diffusible hydrogen measurements by the hot extraction method. Tensile tests were conducted on various weld metals with and without hydrogen charging to evaluate their susceptibility to hydrogen embrittlement. The results show that the carbide-free bainite weld metals are highly resistant to hydrogen embrittlement despite their very high strength.

Introduction

Hydrogen embrittlement of high-strength steel welds is a well-known phenomenon which can lead to premature and catastrophic failures [1]. The combined presence of tensile residual stresses, diffusible hydrogen, and susceptible microstructure is known to cause hydrogen embrittlement [1–3]. The use of low hydrogen welding electrodes, preheating, interpass temperature control, post-heating and post-

* *Corresponding author.*
E-mail addresses: sudharmet@gmail.com (S. Sundaram), jram@msme.iith.ac.in (G.D.J. Ram), murugaiyan@iitm.ac.in (M. Amirthalingam).
https://doi.org/10.1016/j.ijhydene.2023.01.270

weld heat treatments were the conventional methods to overcome the problem of hydrogen embrittlement in steels [4,5]. However, the use of preheating is ineffective or preheating and post-weld heat treatment are not feasible in certain situations. In such circumstances, low-strength austenitic filler wires are used. These filler wires are expensive, can cause hot cracking problems during welding, and often such welds exhibit poor mechanical properties [6,7]. Using hydrogen traps to mitigate hydrogen embrittlement in high-strength steel is being studied extensively [8–12]. The traps are microstructural features where hydrogen resides for either a finite or infinitely long time. Appropriate selection of hydrogen traps can eliminate the problem of hydrogen embrittlement by controlling the diffusion and volume fraction of atomic hydrogen in these trap sites [5]. The presence of austenite and austenite/ferrite interphase boundaries in carbide-free bainite are considered as very effective hydrogen traps. The carbide-free bainite microstructure also exhibits a good combination of strength, ductility, and toughness [13,14].

Escobar et al. [15] compared the hydrogen trapping behaviour of various automotive grade high-strength steels with pure iron as a reference using thermal desorption spectroscopy (TDS), and further correlated the hydrogen trapping behaviour with the mechanical properties. Retained austenite in TRIP steel exhibited hydrogen evolution at elevated temperatures, while other steels showed at lower temperatures. During the tensile test with hydrogen, the steels with higher diffusible hydrogen showed significant ductility loss compared to steels with lesser diffusible hydrogen content. Du et al. [16] analysed the hydrogen diffusivity in low-carbon medium manganese steel containing primarily martensite with varying retained austenite content using the electrochemical permeation technique. It was reported that the hydrogen diffusivity decreases with increase in the volume fraction of retained austenite. Zhou et al. [17] studied hydrogen diffusion and hydrogen trapping of high-strength steel with four different microstructures using the electrochemical permeation technique. Heat treatments were done on a commercial quench and partitioning (Q&P) steel to get a single phase (fully martensitic), two dual phase (martensite + ferrite, martensite + austenite), and a complex phase (martensite + austenite + ferrite) microstructures. The austenite exists as filmy and blocky morphologies in this steel. The study revealed that the interphase boundaries (martensite/austenite, martensite/ferrite, austenite/ferrite) act as reversible traps and lower the hydrogen diffusivity. It was further classified that filmy austenite as a strong reversible trap and blocky austenite as an irreversible trap. Nevertheless, both blocky and filmy austenite increases hydrogen solubility in steel. Du et al. [18] investigated the hydrogen embrittlement susceptibility of low-carbon medium manganese steel with three different volume fractions and the stability of retained austenite in a primarily martensite matrix. The total hydrogen content increases with increase in retained austenite. It was reported that the hydrogen embrittlement susceptibility decreases with increase in retained austenite content and its stability. Brauser and Kannengiesser [19] analysed the hydrogen absorption in two different duplex stainless steel weld metals with varying ferrite and austenite phase fractions. The hydrogen absorbed during the welding process was measured using the hot extraction method and tensile test was carried out to compare the hydrogen embrittlement susceptibility. It was reported that the total hydrogen absorbed during welding was similar but the hydrogen was predominantly weakly trapped in the lower austenite weld metal, and strongly trapped in the higher austenite weld metal. Hydrogen embrittlement was significant in lower austenite weld metal due to weakly trapped hydrogen. Zhu et al. [20] studied Q&P steel with ferrite, martensite, and retained austenite phases. Hydrogen trapping sites analysed using atom probe tomography (APT) revealed that the amount of hydrogen in austenite was three times that of martensite while ferrite exhibited negligible trapping. Hydrogen causes degradation of ductility with cracking initiating from the austenite martensite interfaces. Peet and Hojo [21] studied hydrogen saturation in carbide-free bainite using thermal desorption analysis and correlated hydrogen concentration at saturation to the total surface area of ferrite/austenite interphase boundaries rather than the volume fraction of retained austenite. Szost et al. [22] studied hydrogen trapping of carbide-free bainite using melt extraction and thermal desorption analysis and concluded that hydrogen trapping occurred in ferrite/austenite boundaries and termed such boundaries are reversible traps. Cota et al. [23] studied hydrogen trapping in carbide-free bainite microstructures using thermal desorption analysis. Thermal desorption analysis revealed that retained austenite effectively traps hydrogen than bainitic ferrite/austenite interfaces. A correlation between the amount of hydrogen desorbed after saturation and the volume fraction of retained austenite was obtained. Krishna Murthy et al. [24] suggested carbide-free bainitic fillers as an alternative to conventional austenitic stainless steel fillers for welding armour-grade quenched and tempered steels. It was demonstrated that the carbide-free bainitic weld metal could be obtained in the weld fusion zone by carefully selecting filler metal composition and controlling the welding parameters. The welds showed good weld joint efficiency and cold-cracking resistance.

The effect of hydrogen on mechanical properties was studied by analysing the tensile behaviour of samples with and without hydrogen charging by analysing the reduction in total elongation, cross-sectional area, and tensile strength or fracture strength for notched samples [21,25,26]. However, for high-strength steels, the total elongation or reduction in area is not a useful parameter, as with hydrogen, it fails without any elongation or reduction in area. This leads to ambiguity in results, and therefore delineating the hydrogen effect becomes challenging [27].

Though carbide-free bainite microstructure was studied for hydrogen trapping, contradicting evidence of the effective trapping abilities of its constituent phases exists. The carbide-free bainite microstructure was successfully generated in high-strength steel welds with good cold cracking resistance however, so far detailed study on the influence of microstructural constituents on the hydrogen embrittlement susceptibility of welds is not carried out. In this work, six different carbide-free bainite weld metal samples were generated with varying fractions and morphologies of the constituent microstructural phases, and hydrogen saturation behaviour

and tensile testing of the weld metal samples with and without different levels of hydrogen charging were analysed for hydrogen embrittlement susceptibility. The reduction in ultimate tensile strength due to hydrogen charging is analysed to compare the effect of hydrogen among various weld metals.

Experimental details

Material

Three different alloy compositions, namely alloy A, alloy B, and alloy C were designed, and a detailed study to optimise the welding parameters to get carbide-free bainite weld metal microstructures was reported elsewhere by the authors [28]. Shielded metal arc welding (SMAW) electrodes were manufactured for the designed compositions. Weld deposits were made using the SMAW electrodes on a mild steel substrate for each composition. The schematic of the cross-section of the weld deposit is given in Fig. 1. The weld deposits were made to extract samples for further studies. The chemical composition of the welds is shown in Table 1. The optimised weld thermal cycles for each alloy composition were identified from the previous study [28]. The optimum weld thermal cycle for each alloy involved austenisation at 850 °C for 300 s, followed by cooling to isothermal transformation temperature, held at the temperature for a predetermined time before being cooled to room temperature. The optimum bainitic transformation temperature and time identified for each alloy were (a) Alloy A (A-BT1) - 300 °C, 3 hours; (b) Alloy B (B-BT1) - 300 °C, 2 hours and (c) Alloy C (C-BT2) - 285 °C, 6 hours. The details of the weld thermal cycles are shown in Table 2. The dilatometry analysis was carried out using the above-mentioned thermal cycles in the Gleeble thermomechanical simulator. To study the influence of constituent phases on the hydrogen embrittlement susceptibility, two types of heat treatment were carried out, as shown in Table 2. For each weld metal sample, the holding time required for 50% and near-complete bainitic transformation was identified from the dilatometry curves as shown in Fig. 2. These holding times were applied during the heat treatment of the welds. All the weld metal samples were austenised for 600 s at 850 °C, subsequently transferred to a salt bath furnace for bainitic transformation, and after the bainitic holding time, samples were air-cooled to room temperature. The bainitic transformation temperature and time followed for various weld metal samples were as follows, A-BT1 50–300 °C, 40 minutes; A-BT1 100–300 °C, 3 hours; B-BT1 50–300 °C, 20 minutes; B-BT1 100–300 °C, 2 hours; C-BT2 50–285 °C, 1 hour 35 minutes; C-BT2 100–285 °C, 6 hours; A total of six weld metal samples with varying microstructures were obtained and studied further.

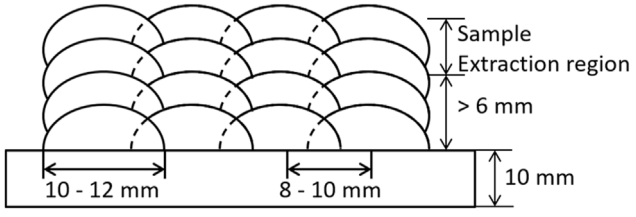

Fig. 1 – Schematic of the cross-section of the weld deposit.

Table 1 – Chemical composition of welds.

	Elements wt.%					
	C	Si	Mn	Ni	Mo	Cr
Alloy A	0.35	1.36	1.9	1.99	0.20	0.03
Alloy B	0.375	1.53	1.63	0.17	0.19	2.23
Alloy C	0.53	1.93	0.96	0.34	0.21	4.23

Characterisation of microstructures

Microstructural characterisation was carried out using scanning electron microscopy (SEM), transmission electron microscopy (TEM), and retained austenite measurement using X-Ray diffraction. For scanning electron microscopy, samples were mechanically polished with a series of emery sheets and cloth polished using 9 μm and 1 μm diamond pastes. Samples were etched with 2 vol % Nital for 10–15 s. SEM analysis was carried out on Apreo S^{TM} equipment in secondary electron imaging mode. For EBSD, samples were prepared similarly to SEM analysis, after polishing with diamond pastes, the samples were polished in colloidal silica for 20 min. For TEM analysis, samples of 250–350 μm were cut using EDM and a thin foil of 80–90 μm was prepared by reducing the thickness using emery sheets. Circular discs of 3 mm diameter were punched out from the samples. Further thinning and perforation at the center of the disc was done by electropolishing on a twin jet polisher (Struers Tenupol-5 twin jet polisher^{TM}) at 25 V for 10 s in a solution consisting of 10 vol % perchloric acid and 90 vol % acetic acid at −30 °C. The samples were examined on JEM F200^{TM} equipment with an accelerating voltage of 200 keV in bright-field imaging mode and selected area diffraction patterns were also obtained for selected samples. Retained austenite was measured using ProtoIXRD^{TM} retained austenite measurement system. Retained austenite was calculated from the integrated intensities of (200), (220) peaks of austenite, and (200), (211) peaks of ferrite. The fractured surface of the tensile specimens was also analysed in the SEM-Apreo S^{TM} equipment in secondary electron imaging mode.

Determination of hydrogen saturation

The hydrogen saturation behaviour of the six different weld metal microstructures was studied by charging the sample with hydrogen using an electrolytic cell and measuring the diffusible hydrogen concentration. For hydrogen charging, samples were used as the cathode, platinum as the anode, and 0.5 M aqueous sulphuric acid solution was used as an electrolyte. To avoid the recombination of hydrogen atoms at the electrode-electrolyte interface, 2 g l^{-1} of thiourea was used as a poisoner. A constant current DC power source was used to maintain a current density of 2 mA cm^{-2}. The hydrogen charging was carried out at room temperature, and the electrolyte was stirred throughout the charging time using a magnetic stirrer. The diffusible hydrogen concentration was measured by the hot extraction method in Bruker G8 Galileo^{TM} ONH analyser. An infrared (IR) furnace was used to heat the

Table 2 – Sample designation and details of heat treatment of the welds.

Description	Alloy Composition	Heat treatment condition	Holding Temperature	Holding time
A-BT1 50	Alloy A	Intermediate bainitic transformation	300 °C	40 minutes
A-BT1 100		Near-complete bainitic transformation		3 hours
B-BT1 50	Alloy B	Intermediate bainitic transformation	300 °C	20 minutes
B-BT1 100		Near-complete bainitic transformation		2 hours
C-BT2 50	Alloy C	Intermediate bainitic transformation	285 °C	1 hour 35 minutes
C-BT2 100		Near-complete bainitic transformation		6 hours

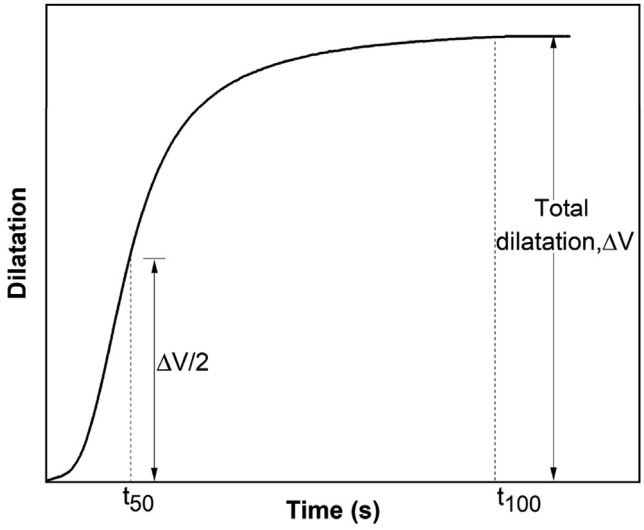

Fig. 2 – Schematic of the dilatation vs time plot of an isothermal bainitic transformation. t_{50} - holding time for 50% transformation; t_{100}-holding time for near-complete transformation.

sample, and a thermal conductivity detector was used in the equipment to measure the hydrogen concentration using nitrogen as carrier gas. Sample dimensions of 15 x 1 x 20 mm^3 were used for the study. Diffusible hydrogen measurements were carried out as per AWS A4.3 standard. After charging, the samples were immediately transferred to ethanol maintained at −80 °C, kept in ethanol for 120 s, then taken out and brought to room temperature by rinsing it in isopropyl alcohol and petroleum ether. The charged samples were subsequently weighed and transferred to the IR furnace for measurements. The cleaning of samples and handling time between samples taken out from ethanol and loading in the IR furnace were maintained at 40–50 s. After each test, the charging time was increased, and the process was repeated until the measured hydrogen values saturated. For each charging time, three tests were carried out and the average value of the three tests was reported. The hydrogen concentration at the saturation level was determined for all six weld metal microstructures.

Determination of hydrogen embrittlement susceptibility

The degradation in the weld metal mechanical properties due to hydrogen charging was analysed by tensile testing. Tensile tests were carried out on an Instron^{TM} 100 kN machine with a video extensometer at a strain rate of 1×10^{-3} s^{-1}. The tensile specimen of 1 mm thick, 3 mm gauge width, and 12 mm gauge length was used. For tensile tests with hydrogen charging, the gauge length alone was exposed to the electrolyte, and other regions were masked using lacquer. After hydrogen charging, the tensile specimen was cleaned in acetone and kept in ethanol maintained at −80 °C. Before the tensile test, the specimen was taken out and brought to room temperature by rinsing it in ethanol and subsequently tested. During the tensile test, cleaning and handling time of 300 s was maintained for all the hydrogen-charged samples. Tensile tests were conducted in uncharged and charged (to saturated level) conditions for all the welds. Further, to study the hydrogen embrittlement susceptibility at the intermediate hydrogen levels, tensile specimens were also charged with 0.25, 0.5, 1, and 2 ppmw of diffusible hydrogen on near-complete transformation weld metal samples. As the handling time between hydrogen charging and the start of the tensile test was 300 s, diffusible hydrogen was measured with a time delay of 300 s. The charging time required to get 0.25, 0.5, 1, and 2 ppmw of diffusible hydrogen in various weld metal samples was determined. The tensile specimens were charged for that predetermined charging time and subsequently tested similarly to other samples. The susceptibility of weld metal against hydrogen embrittlement was evaluated based on the results of these tensile tests by comparing the reduction in ultimate tensile strengths.

Results

The SEM images of six different heat-treated weld metal microstructures are given in Fig. 3. In all the samples, carbide-free bainite was observed along with retained austenite/martensite (RA/M) constituent. The Gleeble dilatometric curves for near-complete bainitic transformed weld metal samples are shown in Fig. 4. In B-BT1 100 it can be noted that martensite formation was not observed upon cooling from the bainitic holding temperature. Except for B-BT1 100, in all samples, martensite is also present along with retained austenite which is not distinguishable in SEM images. In alloy C, near-complete bainitic transformed sample (C-BT2 100), the fraction of retained austenite/martensite constituent was observed to be more in comparison with other near-complete bainitic transformed samples (Fig. 3f), namely A-BT1 100 and B-BT1 100 (Fig. 3b and d respectively). The EBSD phase maps superimposed on the image quality maps for the weld metal samples A-BT1 100, B- BT1 100, and C-BT2 100 are shown in Fig. 5. The blocky austenite was distinctly seen from the bainite ferrite in all these maps. However, the interlath/filmy austenite was not revealed in these maps as the imaging resolution was not sufficiently high.

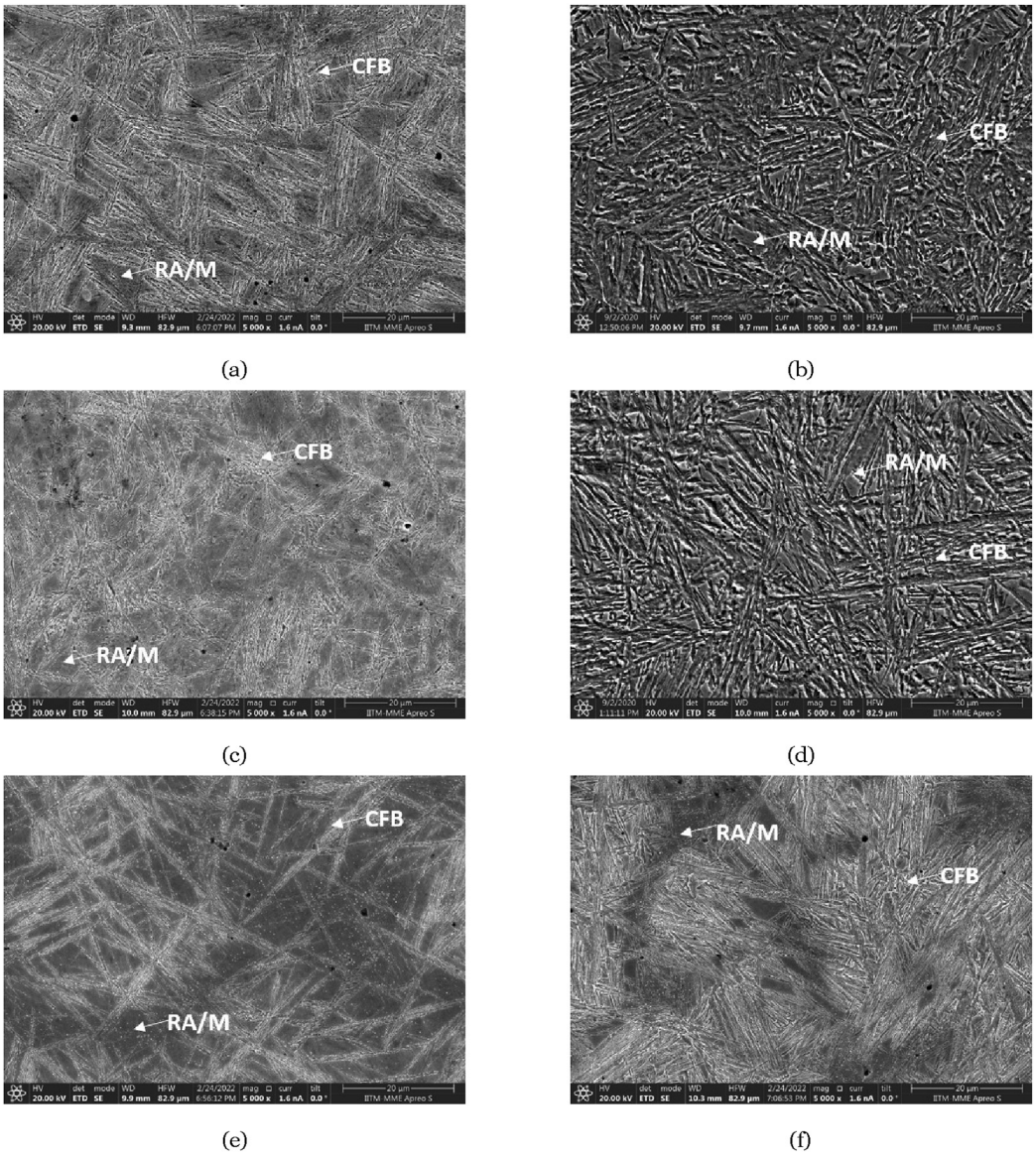

Fig. 3 – SEM images of a) A-BT1 50, b) A-BT1 100, c) B-BT1 50, d) B-BT1 100, e) C-BT2 50, f) C-BT2 100; CFB- carbide-free bainite, RA/M – Retained austenite/Martensite.

The TEM bright-field images of the weld metal microstructures are shown in Fig. 6. The presence of alternate laths of bainitic ferrite and filmy retained austenite was observed in all the samples. The presence of both phases was confirmed by the selected area diffraction pattern of the B-BT1 100 sample as given in Fig. 6g. It was observed that the lath size of bainitic ferrite in alloy C samples (Fig. 6e and f) was smaller in comparison with alloy B (Fig. 6c and d). The lath size of the bainitic ferrite of alloy B samples was finer than alloy A samples (Fig. 6a and b).

Retained austenite measured by the quantitative X-Ray diffraction analysis is shown in Table 3. The retained austenite percentage of alloy A samples was less in comparison with alloy B and alloy C samples. The retained austenite content of the intermediate bainitic transformed sample of alloy A (9 vol %) was slightly higher than the near-complete transformed sample (7 vol %), which was not the case in other alloys. Alloy B showed a significant difference in retained austenite between intermediate (7 vol %) and near-complete bainitic transformed samples (16 vol %).

The diffusible hydrogen concentration of the various weld metal samples as a function of charging time is shown in Fig. 7. The diffusible hydrogen concentration at saturation for the weld metals is given in Table 4. It was observed that the diffusible hydrogen concentration at saturation increases with the increase in retained austenite content. The charging time to saturation was also found to increase with the increase in retained austenite content. Even though A-BT1 50 contains slightly higher retained austenite than B-BT1 50, A-BT1 50 saturated at 4 hours of charging compared with 5 hours of B-BT1 50. C-BT2 50 sample contained significantly higher diffusible hydrogen at saturation in comparison with B-BT1

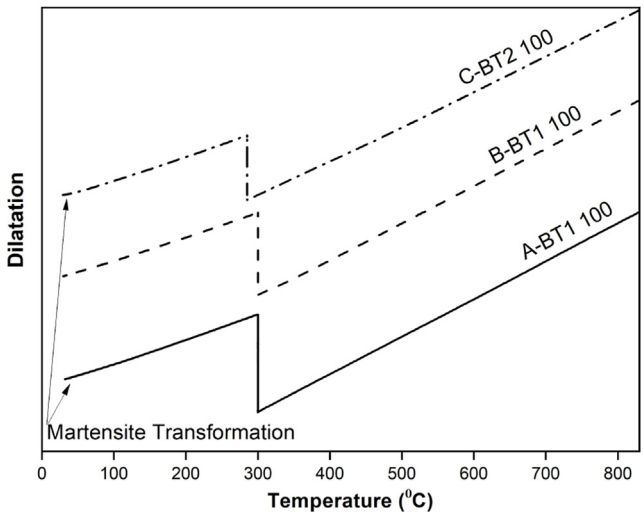

Fig. 4 – Dilatation behaviour of A-BT1 100, B-BT1 100, C-BT2 100 thermal cycles, while cooling from austenisation temperature. Note the absence of martensite transformation in B-BT1 100.

100, although the volume fraction of retained austenite of both samples (16 vol %) was the same. It was also observed that C-BT2 50 showed slightly higher diffusible hydrogen concentration (12.8 ppmw) and lesser charging time to saturation than C-BT2 100 (11.6 ppmw) although the retained austenite volume fraction of C-BT2 100 (18 vol %) was slightly higher than that of C-BT2 50 (16 vol %).

The mechanical properties of heat-treated weld samples with saturated and without hydrogen are shown in Table 5. In uncharged conditions, B-BT1 100 showed a good combination of high strength and ductility among all the samples. Overall, the intermediate bainitic transformed samples showed lesser ductility than the near-complete transformed samples. Except for B-BT1 50, other intermediate transformed samples showed significantly lesser tensile strength than the near-complete transformed samples. With saturated hydrogen charging, the tensile strength of all the samples decreases drastically, and the reduction in tensile strength was more than 50% except for B-BT1 100, which showed a reduction of 43%. In all the samples with saturated hydrogen charging, the samples failed in a brittle manner.

The near-complete transformed samples exhibited better mechanical properties with and without hydrogen charging than the intermediate transformed samples. The tensile behaviour of near-complete transformed samples charged with intermediate levels of hydrogen, namely 0.25, 0.5, 1, 2 ppmw was studied further. The stress-strain curves of the samples are shown in Fig. 8. The tensile properties with intermediate levels of hydrogen for near-complete transformed samples are given in Table 6.

The reduction in tensile strength with hydrogen charging increases with increase in hydrogen concentration in all the samples. However, there was no linear reduction in tensile strength with increase in hydrogen concentration in all the cases. In C-BT2 100 at a lower hydrogen concentration of 0.25 ppmw, the reduction in tensile strength is minimal at 9%. Similarly, the reduction in tensile strength at 0.25 ppmw was more for the A-BT1 100 sample. This can be attributed to the retained austenite content. At 2 ppmw, B-BT1 100 showed the least reduction in tensile strength compared with other samples; moreover, B-BT1 100 showed higher strength than other samples in all hydrogen levels.

SEM images of the fractured surface of both saturated and uncharged tensile samples are shown in Fig. 9. In uncharged tensile specimens of all the weld metals showed evidence of both faceted cleavage features and micro void coalescence. The B-BT1 100 uncharged samples revealed extensive micro void coalescence compared with other samples as given in Fig. 9g. The alloy C uncharged samples showed a minimal micro void coalescence feature than alloy A and alloy B. All the samples that were hydrogen charged to saturation level exhibited predominantly cleavage fracture features.

Discussion

The weld metal microstructures vary in terms of size, morphology, and volume fractions of the phases. In intermediate transformed samples of alloy A, B and C, apart from

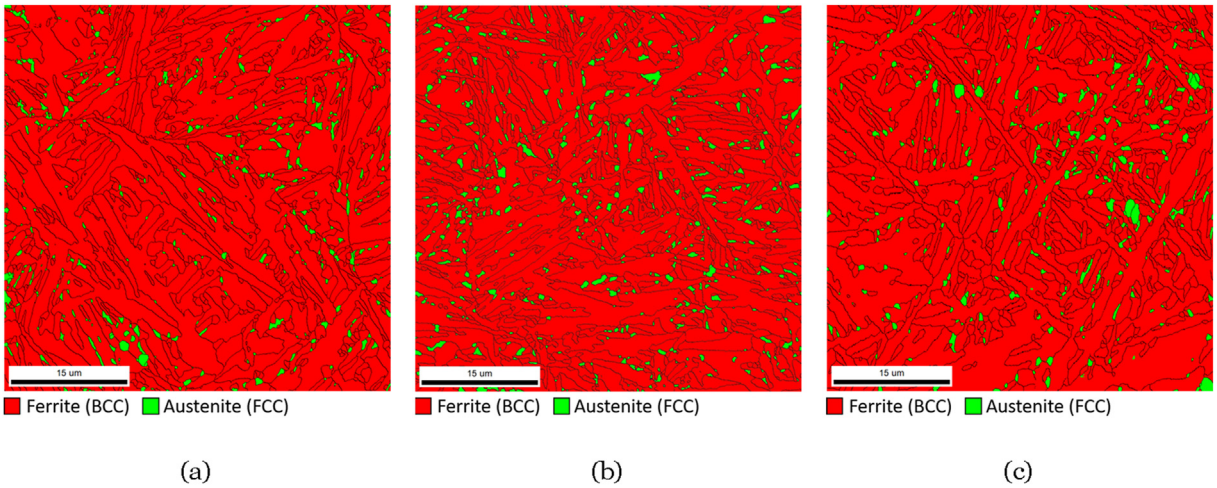

Fig. 5 – EBSD phase map superimposed on the image quality map a) A-BT1 100 b) B-BT1 100 c) C-BT2 100 weld metal samples.

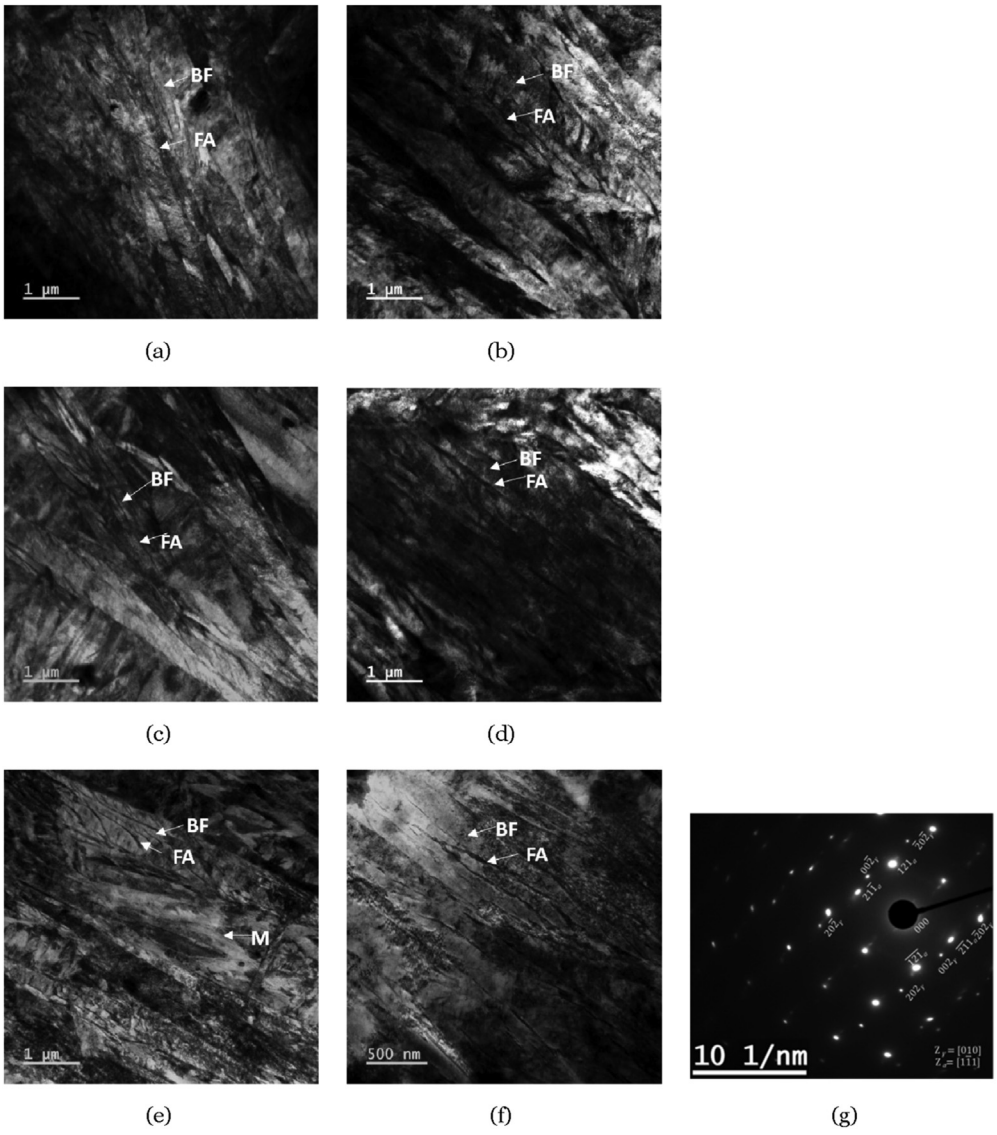

Fig. 6 – TEM images of a) A-BT1 50, b) A-BT1 100, c) B-BT1 50, d) B-BT1 100, e) C-BT2 50, f) C-BT2 100, g) B-BT1 100 DP; FA- filmy interlath austenite, BF- bainitic ferrite.

retained austenite, considerable martensite is also present. Due to partial bainitic transformation, the untransformed austenite is not enriched with carbon enough to stabilise it to room temperature. In near-complete transformed samples, except for B-BT1 100, martensite formed upon cooling from bainitic transformation; this is evident from the Gleeble dilatometry analysis shown in Fig. 4. Despite near-complete transformation to bainite, the carbon enrichment in austenite is not enough to completely avoid martensite transformation in alloy A and C. The carbon enrichment in austenite depends on X_{T_0} (the allotropic phase boundary denoting the carbon concentration at which the Gibbs energies of austenite and bainitic ferrite are equal at a given temperature), which, in turn, is influenced by alloying elements. The volume fraction of martensite formed during cooling depends on the volume fraction of untransformed austenite and the level of carbon enrichment in austenite [29,30]. Though the EBSD phase maps revealed the presence of blocky austenite, the interlath/filmy austenite was not revealed. Hence, the austenite content as measured by EBSD and XRD analyses is not expected to be similar. The volume fraction of blocky austenite in sample B-BT1 100 appeared to be more in comparison to the A-BT1 100 and C-BT2 100. However, SEM studies indicated the amount of blocky austenite is indeed lower in B-BT1 100. More detailed studies are required in this regard.

The TEM images revealed that the bainitic lath size decreases from alloy A to alloy C. This may be due to the difference in carbon content; the presence of carbon effectively increases the strength of the austenite and thereby resists the growth of the bainitic ferrite laths during transformation [31–33]. Substitutional alloying elements also increase the strength of austenite, but the influence of carbon is significant compared with substitutional alloying elements [34,35].

The retained austenite measured using XRD includes both interlath filmy austenite as well as blocky retained austenite.

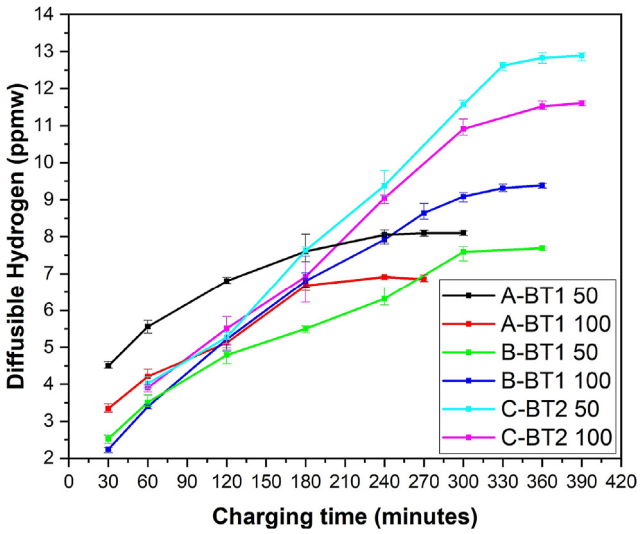

Fig. 7 – Diffusible hydrogen content of weld metals as a function of charging time.

Table 3 – Retained austenite measured using XRD.

Description	Retained austenite Vol. % (±1)
A-BT1 50	9
A-BT1 100	7
B-BT1 50	7
B-BT1 100	16
C-BT2 50	16
C-BT2 100	18

Table 4 – Diffusible hydrogen concentration of the various weld metal samples as a function of charging time.

Description	Hydrogen concentration at saturation (ppmw)
A-BT1 50	8.1 ± 0.09
A-BT1 100	6.9 ± 0.06
B-BT1 50	7.6 ± 0.14
B-BT1 100	9.3 ± 0.11
C-BT2 50	12.8 ± 0.13
C-BT2 100	11.6 ± 0.08

The alloy C contains a higher percentage of retained austenite than other samples due to the higher carbon concentration in alloy C. During transformation, the carbon rejected from the bainitic ferrite saturates the untransformed austenite, once the carbon content reaches the X_{T_0}, the austenite is stabilised. As in alloy C, the overall carbon concentration is higher than other alloys, and the amount of carbon rejected into austenite with the transformation is also higher, which leads to a higher volume fraction of blocky retained austenite [29,36,37]. This is also evident from the SEM images of alloy C, as given in Fig. 3f. The volume fraction of retained austenite in alloy A is lesser than in other alloys due to the reason mentioned above, as carbon concentration in this alloy is less than in other alloys. As the bainitic holding time for the incomplete transformed condition was chosen to have about 50% of bainitic transformation, in these samples, apart from carbide-free bainite and retained austenite, martensite is expected to present as a major constituent. In near-complete transformed samples, martensite is expected not to present as a major constituent as the bainitic transformation was allowed to near completion, as evident from the dilatometry curves in Fig. 4.

The diffusible hydrogen saturation study shows that the amount of diffusible hydrogen increases with increase in retained austenite content. The solubility of hydrogen in austenite is higher than in ferrite and martensite. The diffusivity of hydrogen in austenite is several orders of magnitude lower than that in ferrite and martensite. As a result, austenite serves as an effective trap for hydrogen [38–40]. Hence, the hydrogen concentration at the saturation level increases with increases in austenite content. Moreover, the amount of hydrogen trapped in blocky retained austenite is higher than that trapped in filmy retained austenite for all the alloys. This is particularly well established in alloy C, in which case C-BT2 50 with a lower retained austenite content (16 vol %) showed a higher hydrogen saturation concentration than C-BT2 100 with a higher retained austenite content (18 vol %). In C-BT2 50, the amount of interlath austenite is expected to be nearly half of that in C-BT2 100, and out of all retained austenite, more blocky retained austenite is expected in C-BT2 50. With higher blocky retained austenite in C-BT2 50, the amount of diffusible hydrogen at saturation is also higher compared with C-BT2 100. In Alloy B, even though the retained austenite content in B-BT1 100 is twice that of B-BT1 50, the diffusible hydrogen content in B-BT1 100 is only 25% higher than B-BT1 50. This is

Table 5 – Tensile properties of samples with saturated and without hydrogen.

Description	Condition	UTS (MPa)	0.2% Proof stress (MPa)	Reduction in UTS (%)
A-BT1 50	Uncharged	709 ± 31	705 ± 7	61
	Saturated	273 ± 13		
A-BT1 100	Uncharged	1238 ± 38	1113 ± 31	75
	Saturated	300 ± 19		
B-BT1 50	Uncharged	1674 ± 24	1171 ± 13	78
	Saturated	353 ± 31		
B-BT1 100	Uncharged	1645 ± 26	1078 ± 17	43
	Saturated	934 ± 42		
C-BT2 50	Uncharged	1031 ± 21		61
	Saturated	398 ± 37		
C-BT2 100	Uncharged	1352 ± 16	952 ± 9	54
	Saturated	617 ± 23		

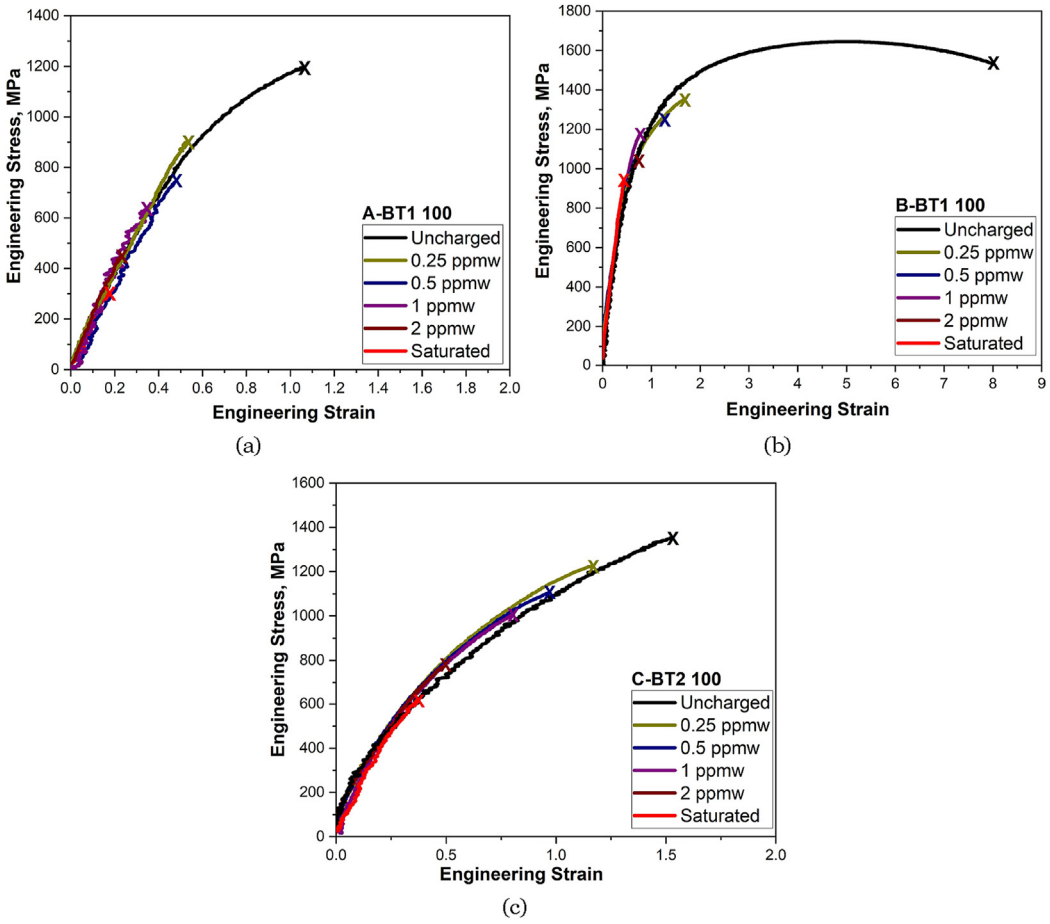

Fig. 8 – Stress-strain curves of weld metal samples with varying diffusible hydrogen contents: a) A-BT1 100 b) B-BT1 100 c) C-BT2 100.

Table 6 – Tensile properties of near-complete transformed samples with varying hydrogen content.

Description	Hydrogen Concentration (ppmw)	UTS (MPa)	Reduction in UTS (%)
A-BT1 100	Uncharged	1113 ± 31	–
	0.25	912 ± 17	27
	0.5	745 ± 26	38
	1	632 ± 12	51
	2	424 ± 27	64
	Saturated (6.9 ± 0.06)	300 ± 19	75
B-BT1 100	Uncharged	1645 ± 26	–
	0.25	1351 ± 27	18
	0.5	1229 ± 21	25
	1	1114 ± 37	32
	2	1017 ± 16	38
	Saturated (9.3 ± 0.11)	934 ± 42	43
C-BT2 100	Uncharged	1352 ± 16	–
	0.25	1225 ± 18	9
	0.5	1051 ± 23	22
	1	985 ± 18	27
	2	802 ± 34	40
	Saturated (11.6 ± 0.08)	617 ± 23	54

also the case explained for alloy C. From the diffusible hydrogen saturation studies, it is also observed that intermediate transformed samples saturate early in comparison with near-complete transformed samples for a given amount of austenite. High dislocation density regions are present in bainitic ferrite near the austenite/ferrite boundaries due to the accommodation of strain during bainitic transformation. Highly dense dislocation regions decrease the diffusivity of hydrogen in bainitic ferrite [41,42]. This explains why the near-complete transformed samples saturate after longer charging times as compared to intermediate transformed samples.

The ultimate tensile strength of carbide-free bainite weld metals predominantly depends on the volume fraction of bainitic ferrite and its lath size. The ductility of the carbide-free bainite microstructure depends on the volume fraction of retained austenite and its stability [43,44]. The interlath filmy retained austenite is more stable than the blocky retained austenite [45–47]. B-BT1 100 weld metal gives high strength and ductility compared with other weld metals. Even though C-BT2 100 has finer carbide-free bainite and higher retained austenite content than B-BT1 100, the strength and ductility of C-BT2 100 are lower than B-BT1 100. This may be due to higher fractions of carbon rich blocky retained austenite observed in C-BT2 100.

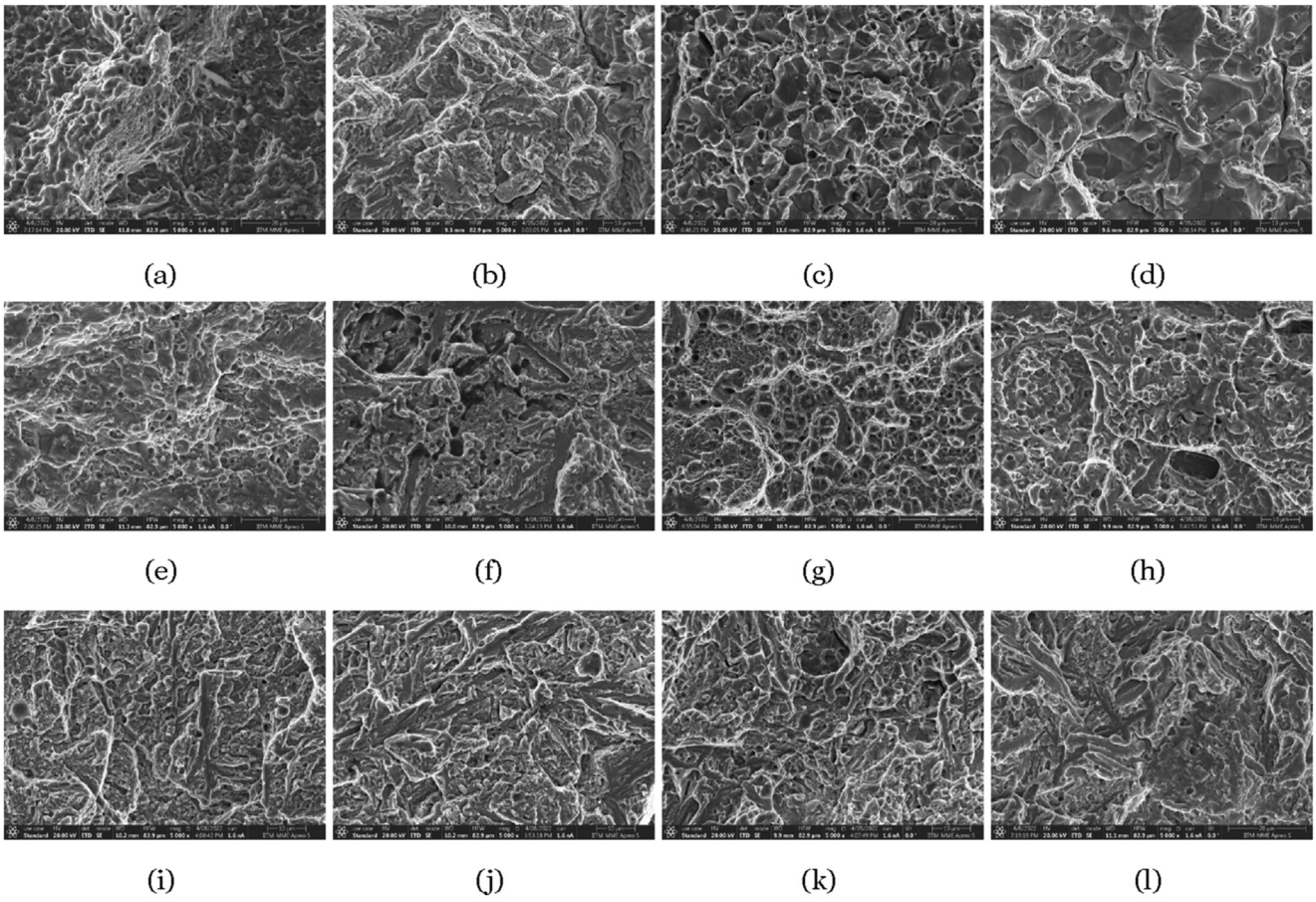

Fig. 9 – SEM images of the fractured surfaces of tensile specimen a) A-BT1 50 uncharged, b) A-BT1 50 saturated, c) A-BT1 100 uncharged, d) A-BT1 100 saturated, e) B-BT1 50 uncharged, f) B-BT1 50 saturated, g) B-BT1 100 uncharged, h) B-BT1 100 saturated, i) C-BT2 50 uncharged, j) C-BT2 50 saturated, k) C-BT2 100 uncharged, l) C-BT2 100 saturated.

With hydrogen saturated samples, the tensile strength dropped drastically, and the presence of unstable blocky retained austenite is found to be an important factor in affecting the strength. The blocky retained austenite transforms to martensite readily upon applied stress. The blocky retained austenite, in general, has a higher carbon concentration than the overall carbon concentration [47–49]. The hydrogen trapped in the blocky retained austenite becomes more diffusible with transformation to martensite, and the diffusivity of hydrogen in the BCC phase is several orders of magnitude higher in comparison with austenite. The inherited diffusible hydrogen and high carbon in the martensite lead to premature brittle failure [14,50,51]. The reduction in tensile strength is less in B-BT1 100 than in other microstructures; this may be due to the presence of more stable interlath austenite, the absence of martensite after bainitic transformation, and a negligible amount of blocky retained austenite as observed in SEM image given in Fig. 3d.

The reduction in tensile strength at intermediate hydrogen content of 0.25–2 ppmw reveals that at low hydrogen concentration of 0.25 ppmw, the presence of blocky retained austenite facilitates retention of tensile strength; this may be due to the fact that 0.25 ppmw is not a critical concentration to cause significant loss in strength [26,52]. With 2 ppmw of diffusible hydrogen, all welds show a significant ductility drop except for B-BT1 100, which is due to the reason explained above for the same microstructure in saturated conditions.

By comparing all the weld metals, it can be summarised that alloy B, B-BT1 100 carbide-free bainite microstructure with the absence of martensite and negligible blocky retained austenite was found to resist hydrogen embrittlement at all hydrogen concentrations.

Conclusions

1. The volume fraction of retained austenite has a direct correlation with the concentration of diffusible hydrogen content in the carbide-free bainitic weld metals.
2. The blocky retained austenite traps more diffusible hydrogen, However, due to its poor mechanical stability, it leads to serious loss in tensile strength.
3. The alloy B, B-BT1 100 carbide-free bainite microstructure with the absence of martensite and negligible blocky retained austenite is better in retaining tensile strength in all hydrogen levels.

Declaration of competing interest

The authors declare that they have no known competing financial interests or personal relationships that could have appeared to influence the work reported in this paper.

Acknowledgement

The authors wish to thank the Science and Engineering Research Board (SERB), Department of Science and Technology, Government of India, for funding Extra Mural Research(EMR) grant (EMR/2016/002755) to carry out this work.

REFERENCES

[1] Hart PHM. First international conference on weld metal hydrogen cracking in pipeline girth welds : 1 2 march 1999, novotel northbeach, wollongong, Australia. The Institute [Lidcombe, N.S.W.; 1999. p. 1.
[2] Yurioka N, Suzuki H. Hydrogen assisted cracking in c-mn and low alloy steel weldments. Int Mater Rev 1990;35:217–49. https://doi.org/10.1179/imr.1990.35.1.217. URL: 10.1179/imr.1990.35.1.217.
[3] Gangloff RP. Hydrogen assisted cracking of high strength alloys. Aluminum Co of America Alcoa Center Pa Alcoa Technical Center; 2003. Technical Report.
[4] Padhy GK, Komizo Y-i. Diffusible hydrogen in steel weldments: a status review. Trans JWRI 2013;42:39–62.
[5] Maroef I, Olson D, Eberhart M, Edwards G. Hydrogen trapping in ferritic steel weld metal. Int Mater Rev 2002;47:191–223. https://doi.org/10.1179/095066002225006548.
[6] Magudeeswaran G, Balasubramanian V, Reddy G. Hydrogen induced cold cracking studies on armour grade high strength, quenched and tempered steel weldments. Int J Hydrogen Energy 2008;33:1897–908. https://doi.org/10.1016/j.ijhydene.2008.01.035.
[7] Kuzmikova L, Norrish J, Li H, Callaghan M. Research to establish a systematic approach to safe welding procedure development using austenitic filler material for fabrication of high strength steel: 16th international conference on the joining of materials. 2011. p. 1–13.
[8] Wei FG, Tsuzaki K. Quantitative analysis on hydrogen trapping of tic particles in steel. Metall Mater Trans 2006;37:331–53.
[9] Lensing C, Park Y, Maroef I, Olson D. Yttrium hydrogen trapping to manage hydrogen in hsla steel welds. Weld J 2004;83:254.
[10] Pound B. Hydrogen trapping in high-strength steels. Acta Mater 1998;46:5733–43.
[11] Jl G, Kd C, Bz B. Delayed fracture properties of 1 500 mpa bainite/martensite dual-phase high strength steel and its hydrogen traps. ISIJ Int 2002;42:1560–4.
[12] Li L, Song B, Cheng J, Yang Z, Cai Z. Effects of vanadium precipitates on hydrogen trapping efficiency and hydrogen induced cracking resistance in x80 pipeline steel. Int J Hydrogen Energy 2018;43:17353–63.
[13] Turnbull A, Hutchings R. Analysis of hydrogen atom transport in a two-phase alloy. Mater Sci Eng 1994;177:161–71.
[14] Bhadeshia HKDH. Prevention of hydrogen embrittlement in steels. ISIJ Int 2016;56:24–36. https://doi.org/10.2355/isijinternational.ISIJINT-2015-430.
[15] Escobar DP, Verbeken K, Duprez L, Verhaege M. Evaluation of hydrogen trapping in high strength steels by thermal desorption spectroscopy. Mater Sci Eng 2012;551:50–8.
[16] Du Y, Gao X, Du Z, Lan L, Misra R, Wu H, Du L. Hydrogen diffusivity in different microstructural components in martensite matrix with retained austenite. Int J Hydrogen Energy 2021;46:8269–84.
[17] Zhou P, Li W, Zhao H, Jin X. Role of microstructure on electrochemical hydrogen permeation properties in advanced high strength steels. Int J Hydrogen Energy 2018;43:10905–14.
[18] Du Y, Gao X, Lan L, Qi X, Wu H, Du L, Misra R. Hydrogen embrittlement behavior of high strength low carbon medium manganese steel under different heat treatments. Int J Hydrogen Energy 2019;44:32292–306.
[19] Brauser S, Kannengiesser T. Hydrogen absorption of different welded duplex steels. Int J Hydrogen Energy 2010;35:4368–74.
[20] Zhu X, Li W, Zhao H, Wang L, Jin X. Hydrogen trapping sites and hydrogen-induced cracking in high strength quenching & partitioning (q& pp) treated steel. Int J Hydrogen Energy 2014;39:13031–40.
[21] Peet MJ, Hojo T. Hydrogen susceptibility of nanostructured bainitic steels. Metall Mater Trans 2016;47:718–25.
[22] Szost BA, Vegter RH, Rivera-Díaz-del Castillo PE. Hydrogen-trapping mechanisms in nanostructured steels. Metall Mater Trans 2013;44:4542–50.
[23] Cota A, Ooi S, Solano-Alvarez W, Bhadeshia H. Infusion of hydrogen into nanostructured bainitic steel. Mater Char 2017;134:96–102.
[24] Krishna Murthy N, Janaki Ram G, Murty B, Reddy G, Rao T. Carbide-free bainitic weld metal: a new concept in welding of armor steels. Metall Mater Trans B 2014;45:2327–37.
[25] Akiyama E, Wang M, Li S, Zhang Z, Kimura Y, Uno N, Tsuzaki K. Studies of evaluation of hydrogen embrittlement property of high-strength steels with consideration of the effect of atmospheric corrosion. Metall Mater Trans 2013;44:1290–300.
[26] Lee J, Lee T, Mun D-J, Bae CM, Lee CS. Comparative study on the effects of cr, v, and mo carbides for hydrogen-embrittlement resistance of tempered martensitic steel. Sci Rep 2019;9:1–9.
[27] Lovicu G, Bottazzi M, D'aiuto F, De Sanctis M, Dimatteo A, Santus C, Valentini R. Hydrogen embrittlement of automotive advanced high-strength steels. Metall Mater Trans 2012;43:4075–87.
[28] Sundaram S, Ram G, Amirthalingam M. Development of shielded metal arc welding electrodes to achieve carbide-free bainitic weld microstructures. Weld World 2021;65:1–11.
[29] Bhadeshia H, Edmonds D. Bainite in silicon steels: new composition–property approach part 2. Met Sci 1983;17:420–5.
[30] Garcia-Mateo C, Paul G, Somani MC, Porter DA, Bracke L, Latz A, Garcia De Andres C, Caballero FG. Transferring nanoscale bainite concept to lower c contents: a perspective. Metals 2017;7:159.
[31] Soliman M, Palkowski H. Ultra-fine bainite structure in hypo-eutectoid steels. ISIJ Int 2007;47:1703–10.
[32] Singh S, Bhadeshia H. Estimation of bainite plate-thickness in low-alloy steels. Mater Sci Eng 1998;245:72–9.
[33] Wang X, Wu K, Hu F, Yu L, Wan X. Multi-step isothermal bainitic transformation in medium-carbon steel. Scripta Mater 2014;74:56–9.
[34] Bhadeshia HKDH. Bainite in steels: theory and practice. CRC Press; 2019.
[35] Garcia-Mateo C, Caballero FG, Sourmail T, Cornide J, Smanio V, Elvira R. Composition design of nanocrystalline bainitic steels by diffusionless solid reaction. Met Mater Int 2014;20:405–15.

[36] Caballero FG, Santofimia MJ, Capdevila C, García-Mateo C, De Andrés CG. Design of advanced bainitic steels by optimisation of ttt diagrams and t0 curves. ISIJ Int 2006;46:1479–88.
[37] Caballero F, Santofimia M, García-Mateo C, Chao J, De Andres CG. Theoretical design and advanced microstructure in super high strength steels. Mater Des 2009;30:2077–83.
[38] Laureys A, Depover T, Petrov R, Verbeken K. Characterization of hydrogen induced cracking in trip-assisted steels. Int J Hydrogen Energy 2015;40:16901–12.
[39] Dwivedi SK, Vishwakarma M. Effect of hydrogen in advanced high strength steel materials. Int J Hydrogen Energy 2019;44:28007–30.
[40] Pinson M, Springer H, Depover T, Verbeken K. The effect of quench cracks and retained austenite on the hydrogen trapping capacity of high carbon martensitic steels. Int J Hydrogen Energy 2021;46:16141–52.
[41] Fielding L, Song EJ, Han D-K, Bhadeshia H, Suh D-W. Hydrogen diffusion and the percolation of austenite in nanostructured bainitic steel. Proc Math Phys Eng Sci 2014;470:20140108.
[42] Kazum O, Beladi H, Timokhina IB, He Y, Bobby Kannan M. Hydrogen permeation in nanostructured bainitic steel. Metall Mater Trans 2016;47:4896–903.
[43] Kumar A, Singh A. Mechanical properties of nanostructured bainitic steels. Materialia 2021;15:101034.
[44] Garcia-Mateo C, Caballero F. Ultra-high-strength bainitic steels. ISIJ Int 2005;45:1736–40.
[45] Garcia-Mateo C, Caballero FG. Design of carbide-free low-temperature ultra high strength bainitic steels. Int J Mater Res 2007;98:137–43.
[46] Garcia-Mateo C, Caballero FG, Sourmail T, Smanio V, de Andres CG. Industrialised nanocrystalline bainitic steels. design approach. Int J Mater Res 2014;105:725–34.
[47] Timokhina I, Hodgson P, Pereloma E. Effect of microstructure on the stability of retained austenite in transformation-induced-plasticity steels. Metall Mater Trans 2004;35:2331–41.
[48] Caballero F, Bhadeshia H. Very strong bainite. Curr Opin Solid State Mater Sci 2004;8:251–7.
[49] Pereloma E, Timokhina IB, Miller MK, Hodgson PD. Three-dimensional atom probe analysis of solute distribution in thermomechanically processed trip steels. Acta Mater 2007;55:2587–98.
[50] Park Y, Maroef I, Landau A, Olson D. Retained austenite as a hydrogen trap in steel welds. Welding Journal-New York 2002;81:27 [S.].
[51] Ryu JH, Chun YS, Lee CS, Bhadeshia H, Suh DW. Effect of deformation on hydrogen trapping and effusion in trip-assisted steel. Acta Mater 2012;60:4085–92.
[52] Namboodhiri TG. Hydrogen embrittlement of metallic materials. Trans Indian Inst Met 1984;37:764–93.